ACS APPLIED MATERIALS & INTERFACES

Article

Fabrication of novel electrochemical biosensor based on graphene nanohybrid to detect H2O2 released from living cells with ultrahigh performance

Tingting Zhang, Yue Gu, Cong Li, Xiaoyi Yan, Nannan Lu, He Liu, Zhiquan Zhang, and Hong Zhang

ACS Appl. Mater. Interfaces, **Just Accepted Manuscript** • DOI: 10.1021/acsami.7b14029 • Publication Date (Web): 12 Oct 2017

Just Accepted

ACS Publications

ACS Applied Materials & Interfaces is published by the American Chemical Society.
1155 Sixteenth Street N.W., Washington, DC 20036

Fabrication of novel electrochemical biosensor based on graphene nanohybrid to detect H_2O_2 released from living cells with ultrahigh performance

Tingting Zhang[a], Yue Gu[a], Cong Li[a], Xiaoyi Yan[a], Nannan Lu[a], He Liu[a], Zhiquan Zhang[a], Hong Zhang[b]**

[a] College of Chemistry, Jilin University, Changchun 130012, China

[b] Department of Physiology, College of Basic Medical Sciences, Jilin University, Changchun 130021, China

KEYWORDS: graphene; hybrid material; electrochemical; H_2O_2; living cell

ABSTRACT: In this paper, a new class of metal-free nanocarbon catalyst — nitrogen (N) and sulfur (S) co-doped graphene quantum dot/graphene (NS-GQD/G) hybrid nanosheets were designed and synthesized for sensitive detection of hydrogen peroxide (H_2O_2). NS-GQD/G was prepared through two steps. Firstly, graphene quantum dots (GQDs) were self-assembled on graphene nanoplatelets via hydrothermal treatment to constitute hybrid nanosheets, followed by a thermal annealing procedure using the hybrid nanosheets and thiourea to form the NS-GQD/G hybrid nanosheets. This hybrid material possessed high specific surface area, numerous doping sites and edges, and high electrical conductivity, which leads to ultrahigh performance toward H_2O_2 electrocatalysis reduction. Under the optimal experimental conditions, the proposed H_2O_2 sensor displayed an extended linear response in the range from 0.4 μM to 33 mM with a low detection limit of 26 nM (S/N = 3). In addition to desirable selectivity, ideal reproducibility, and long-time stability, this H_2O_2 sensor exhibited desirable performance in detecting H_2O_2 in the

human serum samples and that released from Raw 264.7 cells. Therefore, the novel NS-GQD/G nanocomposite was a promising metal-free material in the fields of electrochemical sensing and bioanalysis.

1. INTRODUCTION

H_2O_2 plays pivotal roles in industrial, fuel cells, environmental protection, pharmaceutical, and many other fields[1-4]. Peculiarly, H_2O_2 is closely related to cell growth and signal transduction, and it is recognized as a biomarker in living cells for cancer diagnostics due to its concentration level is a critical physiological parameter for diseases research such as myocardial infarct, Alzheimer's disease, Parkinson's disease, cancer[5-7]. In view of the practical meaning of H_2O_2 in biological systems, exploiting efficient and dependable techniques to sensitively and selectively detect H_2O_2 is to a great extent crucial to avoid lethal attacks of oxidative stress, neurodegenerative disease, and cancer growth.[8]

To date, in contrast with typical techniques for H_2O_2 detection consisting of spectrophotometry [9-10], fluorescence [11-12], chemiluminscence [13], chromatography [14-15], and phosphorescence [5], electrochemical technique is getting a lot of well-deserved attention recently owing to its inherent advantages containing cost-efficient, simple operation, quick determination, high sensitivity, and excellent selectivity [16-17]. Representative electrochemical method, using enzyme-based sensors to disclose H_2O_2, has attracted considerable attention in virtue of its high sensitivity and specificity under certain physiological conditions[18-19]. Nevertheless, enzyme-based electrochemical sensors suffer from intrinsic drawbacks including high cost

preparation procedures, enzyme degeneration [20], and environmental instability [21], which restricts their practical application in H_2O_2 determination. As a consequence, extensive researches have been devoted to enzymeless electrochemical sensors that have high stability and wide application range. Nonenzymatic H_2O_2 sensors are diametrically based on H_2O_2 electrooxidation and electroreduction, thus developing new electrode materials with high catalytic activity and catalytic stability is of the utmost importance.

Heteroatoms doping into the carbon nanomaterials could availably adjust their inherent performance including surface trait, electronic feature, and local chemical characteristic [22-23]. For instance, the metal-free "graphene alloy" — heteroatom-doped graphene, a typical two-dimensional (2D) nanocarbon material based on graphene, has aroused general interest among different fields [24]. With fractional carbon atoms superseded by one or more species of heteroatoms, such as N, P, S, B, Cl and F, the metal-free "graphene alloy" displays remarkably superior electrocatalytic activity than un-doped counterparts. The reason behind this is that with heteroatoms introduced into graphene sheets, the "graphene alloy" could possess even more abundant effective surface areas, plenty active sites, high free charge-carrier densities, and enhanced conductivity. In addition, the interactions between doped graphene and other nanoparticles molecules or nanoparticles get strengthened. Owing to the fact that the metal-free "graphene alloy" offers good performance such as low-cost, high electrocatalytic activity, favorable selectivity, and superior stability [25], the "graphene alloy" has been smoothly used in the applications of lithium-ion batteries [26],

supercapacitors [27], fuel cells [28], and electrochemical sensors [29]. Further, experimental studies concentrated on heteroatoms-doping have proved that co-doping graphene with two kinds of heteroatoms can successfully bring about even more catalytic active sites than singularly doped counterparts as the result of synergistic coupling effects between the doped heteroatoms [30]. The synergistic effects could give rise to a larger asymmetrical spin and higher charge density than that caused by singular doping [31]. For example, Xu *et al.* proved that the dual-doped catalyst, N and S heteroatoms co-doped graphene (NS-G), exhibited considerably superior catalytic activity than mono N-doped or S-doped graphene [32].

Lately, GQDs, a new sort of zero-dimensional (0D) nanocarbon material based on graphene, have become a hot research spot. In contrast to graphene, GQDs display new characters as a result of edge effects and quantum confinement. The edge effects property of GQDs is propitious to boost its electrocatalytic activity since electrocatalytic reactions are apt to take place at edge planes[33-34]. Owing to its superior photostability, outstanding biocompatibility, high catalytic activity, convenient surface modification and functionalization, GQDs have been smoothly applied in photovoltaic devices, biological imaging, catalysts, and electrochemical sensors [35-36]. Heteroatom-doped GQDs, similar to heteroatom-doped graphene, have been demonstrated to have advanced electrocatalytic activity than undoped counterparts. Li's group reported that N doped GQDs (N-GQDs) showed improved electrocatalytic activity to the oxygen reduction reaction (ORR), since doping N atoms into GQDs matrix could furnish more active sites and drastically change their

electronic characteristics [37].

Recent researches have demonstrated that the GQDs present peroxidase-like activity to the reduction of H_2O_2 as a result of plenty aromatic structure and rich periphery carboxylic groups [38-39]. Consequently GQDs are probable to be employed for constructing H_2O_2 electrochemical sensors. In order to further boost the electrical conductivity and electrocatalytic reduction performance of GQDs toward H_2O_2, we combined GQDs with graphene oxide (GO) through hydrothermal self-assembly to obtain graphene quantum dot/graphene (GQD/G) nanosheets. Afterwards, GQD/G nanosheets were thermal annealed with thiourea to acquire NS-GQD/G hybrid nanoflakes. In this paper, we for the first time utilized NS-GQD/G hybrid nanoflakes as sensing platform to exploit a sensitive and selective H_2O_2 electrochemical sensor. The mental-free NS-GQD/G nanosheets based electrochemical sensor exhibited superior electrocatalytic activity toward H_2O_2 reduction, and it could be utilized to sensitively and selectively detect H_2O_2 in human serum and H_2O_2 that released from live cells. Furthermore, NS-GQD/G based electrochemical sensor was prospective to be applied in physiological and pathological researches.

2. EXPERIMENTAL SECTION

2.1. Reagents and materials. Natural graphite came from Qingdao Hengrui Industrial, China. Thiourea was acquired from Xilong Chemical Co., China. H_2O_2, concentrated sulfuric acid (H_2SO_4, 98%), potassium permanganate ($KMnO_4$), disodium hydrogen phosphate (Na_2HPO_4) and potassium dihydrogen phosphate (KH_2PO_4) were obtained from Beijing Chemical Factory, China. Catalase was purchased from Beijing Coolaber Technology Co., China. All chemicals were of

analytical grade and used as received without further purification. Doubly distilled water was used throughout this research. The human blood serum was acquired from The First Hospital of Jilin University, Changchun. The 0.1 M phosphate buffer solution (PBS, pH = 7.0) was produced via dissolving Na_2HPO_4 and KH_2PO_4 in doubly distilled water, and 0.2 M NaOH was applied to regulate and control the final pH value. All experiments were conducted at room temperature.

2.2. Apparatus. Scanning electron microscopy (SEM) measurements were obtained by employing of JEOL JSM 6700F scanning electron microscope operated at 5 kV acceleration voltage. Fourier transform infrared spectroscopy (FTIR) images were achieved with a Nicolet Impact 410 FTIR spectrometer. Transmission electron microscopy (TEM) experiments were carried out on a Philips-FEI Tecnai G2S-Twin microscope with an acceleration voltage of 200 kV. Powder X-ray diffraction (XRD) analysis was performed on a Rigaku D/Max 2550 X-ray diffractometer using Cu Kα radiation (λ =1.5418 Å). X-ray photoelectron spectroscopy (XPS) measurements were conducted on an ESCALAB-MKII 250 X-ray photoelectron spectrometer adopting Al Kα radiation.

Electrochemical measurements were conducted on a CHI 920C electrochemical workstation (CH Instruments, Shanghai Chenhua Instrument Co., China) equipped with a conventional three-electrode cell. The common three-electrode cell includes a working electrode, a reference electrode and a counter electrode. In this research, a bare glassy carbon electrode (GCE, 3 mm in diameter) or a nanocarbon material modified GCE was exploited as working electrode, a saturated calomel electrode (SCE) was exploited as reference electrode, and a platinum wire was exploited as counter electrode. All potentials mentioned in this paper were referenced to SCE.

2.3. Preparation of NS-GQD/G

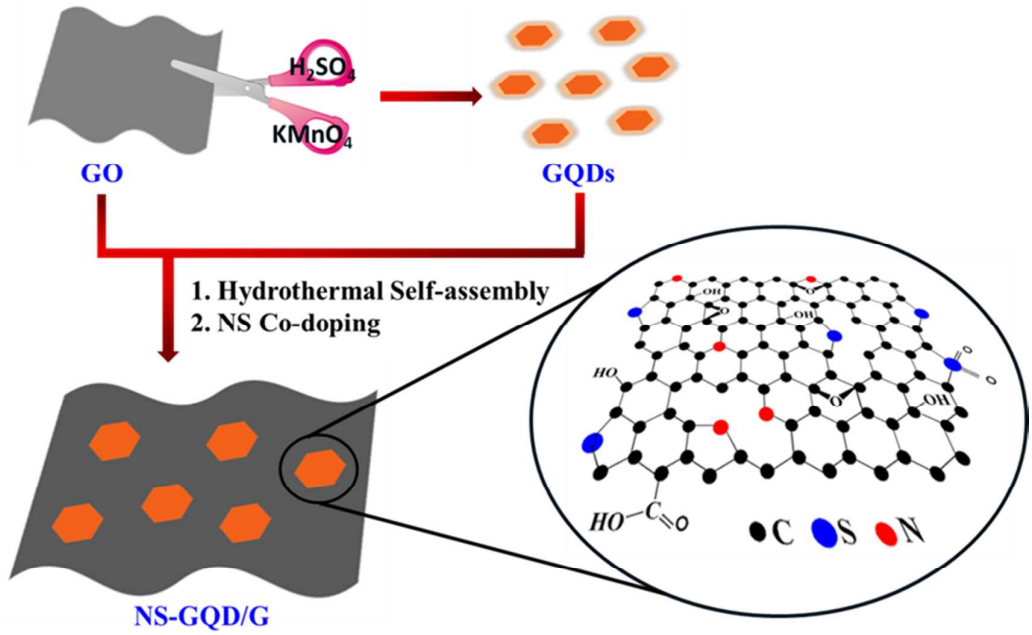

Scheme 1. The schematic illustration of the preparation procedure for the NS-GQD/G nanocomposite

Prior to the synthetize of NS-GQD/G nanosheets, GO and GQDs were firstly prepared and verified, and the details can be found in the Supporting Information. Typically, NS-GQD/G can be synthetized by two processes: first fabricating GQD/G nanosheets and then co-doping GQD/G with N and S atoms, as illustrated in Scheme 1. GQD/G nanoflakes were manufactured through a hydrothermal procedure. Generally, 20 mg GQDs and 10 mg GO were mixed with 15 mL doubly distilled H_2O via being sonicated for 2 h. After that, the obtained aqueous suspension was poured into a 20 mL Teflon-lined autoclave, and then heated for 14 h at the temperature of 180 °C. The obtained aqueous solution was centrifuged at 8000 rpm for 6 min in order to get solid precipitate. At last, the obtained GQD/G product was dried in a vacuum oven at 60 °C for 14 h.

The co-doping process was carried out by thermal annealing GQD/G hybrid nanosheets with thiourea. In a typical synthesis, 20 mg of previously obtained GQD/G

powders were adequately mixed with 200 mg of thiourea via grinding with mortar and pestle. Then, the GQD/G and thiourea mixture was shifted to a quartz boat and heated in a tubular furnace. The temperature was increased to 800 °C at the heating rate of 5 °C min^{-1} and kept at 800 °C for 40 min. The thermal annealing process was conducted under N_2 atmosphere with a flow rate of 10 mL min^{-1}. After that, the resultant NS-GQD/G composite was washed with H_2O for 3 times by centrifugation to remove residual thiourea, and then dried in a vacuum oven at 60 °C for 20 h. By contrast, NS-G was fabricated via the same process, but the GQDs were absent through the hydrothermal procedure. In addition，the un-doped graphene was also obtained through similar step without GQDs and thiourea.

2.4. Preparation of the NS-GQD/G modified electrodes and electrochemical detection of H_2O_2. Before fabricating modified electrode, the bare GCE needs to be polished using 0.3, and 0.05 μm alumina powder to get a specular surface, then sonicated respectively for 1 min in nitric acid/water (1/1, v/v), absolute alcohol, and secondary distilled water. Subsequently, the cleaned electrode was dried under nitrogen steam. For the purpose of constructing NS-GQD/G modified electrodes, 1 mg of NS-GQD/G catalyst was uniformly dissolved in 1 mL of water by sonicating in an ultrasonic bath for 2 h. Then, 15 μL of NS-GQD/G suspension (1.0 mg mL^{-1}) was cautiously cast onto the surface of a newly polished GCE, and the electrode was dried in the air at room temperature. Accordingly, the NS-GQD/G modified GCE (NS-GQD/G/GCE) was successfully prepared. For controlled experiments, 15 μL of NS-G suspension, GQDs solution, and graphene suspension of same concentration (1.0 mg mL^{-1}) were also modified on the same GCE separately via the same experiment steps. The obtained modified electrodes were respectively denoted as NS-G/GCE, GQD/GCE and G/GCE.

2.5. Detection of H_2O_2 in Living Cells. Raw 264.7 cells were cultured in 75 cm^2 flasks containing Dulbecco's modified Eagle's medium supplemented with 10% (v/v) fetal bovine serum (FBS) and 1% antibiotics in an incubator under the condition of 5% CO_2 and 37 °C. Raw 264.7 cells were centrifuged for collection and washed three times using PBS to get rid of incubation solution. Raw 264.7 cells were resuspended into 6 mL of deoxidized PBS (0.1 M, pH = 7.0) for the amperometric detection of H_2O_2 released from Raw 264.7 cells. After the background noise was steady, 10 μL of CdTe QDs (2.0 mg mL^{-1}, synthesised by refluxing routes with mercaptopropionic acid (MPA) as stabilizer[40]) were injected into the PBS to stimulate cells to generate H_2O_2 and then 50 μL of catalase (2000 U mL^{-1}) was added to decompose H_2O_2, the corresponding electrochemical responses were recorded by amperometric *i-t* curves.

3. RESULTS AND DISCUSSION

3.1. Characterization of the NS-GQD/G hybrid nanosheets. Figure 1a exhibited the representative X-ray diffraction (XRD) profiles of resulted materials. As shown, GO displayed an intense and sharp diffraction peak at $2\theta \approx 10.5°$ with a d-spacing of 0.84 nm. After hydrothermal treatment and thermally annealing procedure, GO was effectively transformed to graphene accompanied by the complete vanish of the diffraction peak at $2\theta \approx 10.5°$ and the appearance of a comparatively wider peak centered at $2\theta \approx 22.6°$. In the case of NS-G and NS-GQD/G, broad diffraction peaks at $2\theta \approx 26.2°$ were observed, which were considerably higher than that of graphene, indicating smaller interlayer spacing of NS-G and NS-GQD/G. This tight interlayer spacing might result from the effective π–π stacking of tiny graphenes with few structural defects as N and S doping could induce more topological defects. In addition, compared to NS-G, NS-GQD/G showed a much broader diffraction peak, demonstrating that the introducing of GQDs could bring about more active sites on

the NS-GQD/G surface [41].

XPS was performed to study the surface chemical states and electronic binding states of various atomic species. The XPS survey spectra (Figure 1b) of NS-G and NS-GQD/G showed two predominant peaks associated with C 1s and O 1s electrons as well as two minor peaks associated with N 1s and S 2p electrons, indicating the presence of N and S dopants in the materials. The N and S contents in NS-GQD/G were 5.47 and 2.96 at.%, which were relatively higher than that of NS-G (2.51 and 0.74 at.%, respectively). This was because the decoration of GQDs could permit easy incorporation of dopants owing to sufficient exposed edges and oxygen-containing functional groups in GQDs. Besides, the O 1s peak of NS-GQD/G was visibly stronger than that of NS-G as a result of the addition of GQDs. Furthermore, compared with GO, the significant decrease of the O 1s peak of NS-G and NS-GQD/G obviously confirmed the successful reduction of GO through synthetic reaction. The N 1s spectrum (Figure 1c) was deconvoluted into three peaks assignable to pyridinic N (398.4 eV), graphitic N (401.1 eV) and oxidized N (403.9 eV) species. The graphitic N and pyridinic N, which were widely considered to play an important part in catalytic activities, accounted for the majority proportion of the N species. The S2p spectrum was also deconvoluted to investigate its chemical states. As displayed in Figure 1d, two intense peaks appeared at 164.2 and 165.8 eV were related to thiophenic sulfur, as well as a weak peak (167.9 eV) associated with oxidized sulfur. Abounded thiophenic sulfur affirmed that S atoms were smoothly doped into graphene defects sites and edges, which was highly beneficial for enhancing the electrocatalytic performance of graphene.

The morphology and structure of the synthesized NS-G and NS-GQD/G hybrid nanosheets was investigated via SEM. As illustrated in Figure 1e and 1f, both NS-G

and NS-GQD/G hybrid nanoplates exhibited extremely crinkled and curved structure in contrast with graphene (Figure S1b), which ascribed to the incorporation of N and S atoms into graphene matrixs. Furthermore, the surface of NS-GQD/G was observed to be rougher in comparation with that of NS-G as the result of the decoration of particle-like GQDs on the NS-G sheets. The crinkled and rougher morphology made NS-GQD/G maintain high specific surface area. Additionally, the consequent loosely packed NS-GQD/G matrixs accompanied by plentiful voids accelerated the approach for electrolyte to the catalytic surface, which boosted its electrochemical property.

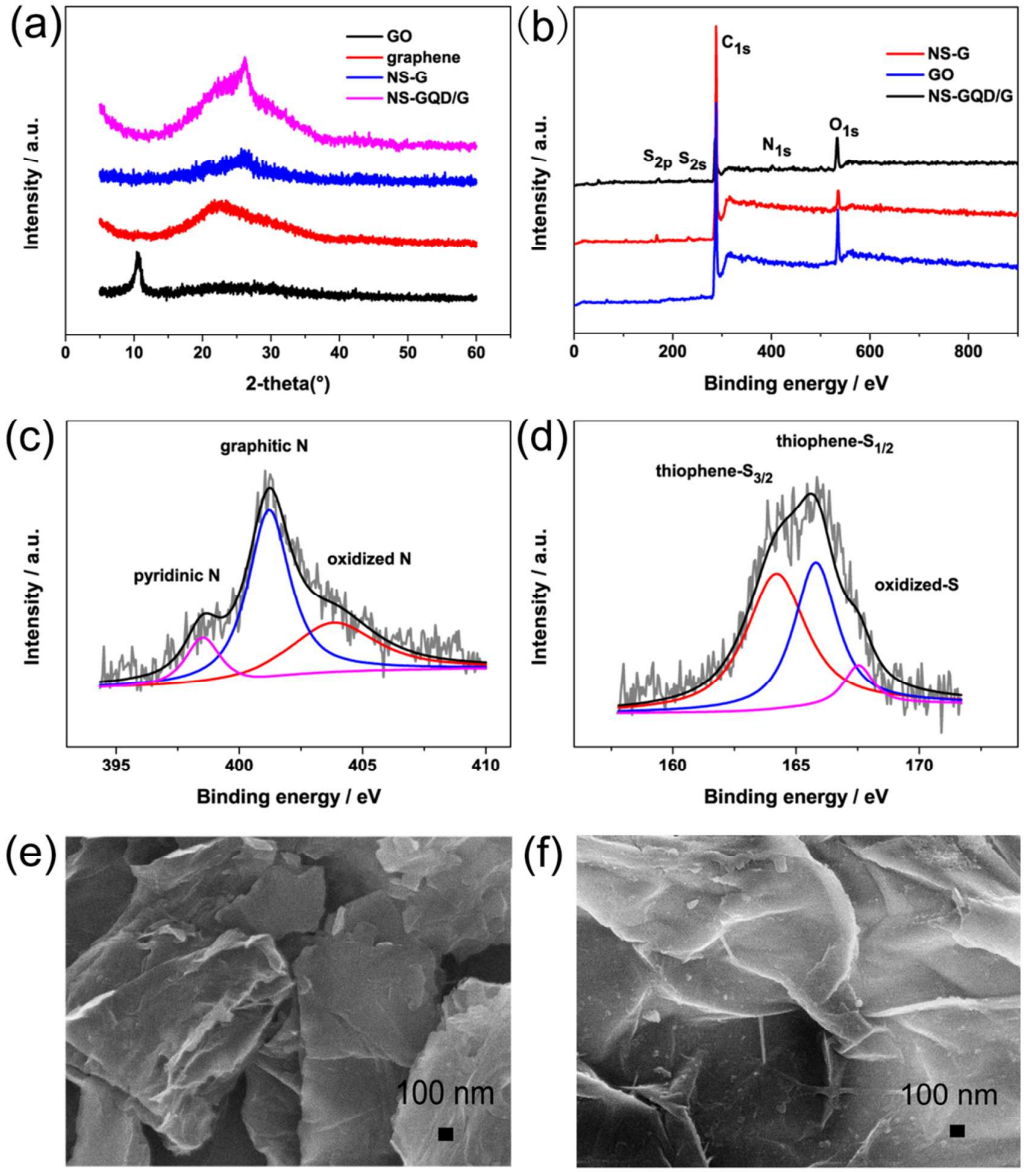

Figure 1. (a) XRD patterns of GO, graphene, NS-G and NS-GQD/G. **(b)** XPS survey scan of NS-GQD/G. High-resolution N1s **(c)** and S2p **(d)** spectrum of NS-GQD/G. SEM images of NS-G **(e)** and NS-GQD/G **(f)**.

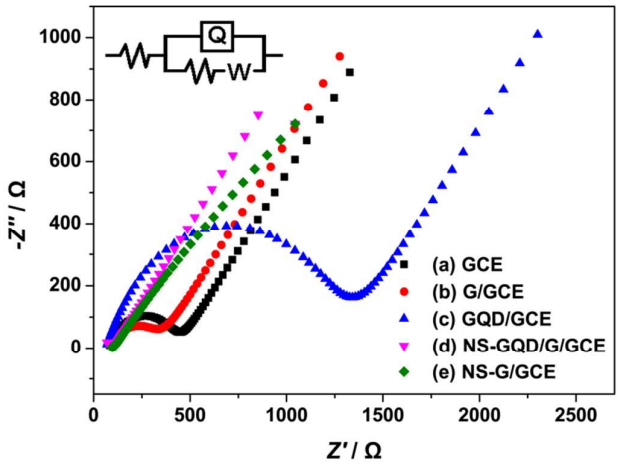

Figure 2. EIS curves of GCE, G/GCE, GQD/GCE, NS-GQD/G/GCE, and NS-G/GCE in 0.1 M KCl solution containing 10 mM $K_3[Fe(CN)_6]/K_4[Fe(CN)_6]$ (1:1). The frequency range of EIS was from 10^5 to 0.01 Hz with the amplitude of 5 mV. The inset is the equivalent circuit.

The electron transfer behaviors and the surface character of NS-GQD/G nanocomposite were probed by electrochemical impedance spectroscopy (EIS). The EIS tests were conducted via employing 0.1 M KCl and 10 mM $K_3[Fe(CN)_6]/K_4[Fe(CN)_6]$ (1:1) solution as the background electrolyte. The measured EIS were fitted applying the classical Randles electronic equivalent circuit and displayed in Figure 2. In accordance with the traditional Faradic impedance spectra, the obtained EIS were composed of a semicircle portion and a straight line portion respectively at higher and lower frequencies. The semicircle portion was bound up with electron transfer-limited course and the straight line portion was related to diffusion-limited procedure. The diameter of semicircle in EIS indicates the charge transfer resistance (R_{ct}) at the electrode surface [42]. For the bare GCE, the R_{ct} value was scaled to be 366.3 Ω. After the bare GCE was modified with graphene, the electrochemical impedance declined to 320.2 Ω, denoting that graphene could accelerate electron transfer between the electrode surface and $[Fe(CN)_6]^{3-/4-}$

electrochemical probe. Furthermore, when the graphene was co-doped with N and S heteroatoms, the electrochemical impedance exceedingly decreased to 38.33 Ω, which verified the introducing of heteroatoms into graphene matrix could accelerate electron transfer rate. This result showed good agreement with previous researches concerning electrical conductivity of N and S atoms doped graphene. Researches indicated that N and S atoms could serve as electron donors, and thus give rise to boosted charge-carrier concentration and improved carbon matrix conductivity [43-44]. The GQD/GCE demonstrated a R_{ct} value of 1240 Ω, indicating that the electroconductivity of GQDs was inferior to graphene. This may be because the small size of GQDs hindered the formation of an adequate percolative network for favorable electroconductivity [45]. Interestingly, the R_{ct} value of NS-GQD/G/GCE (103.0 Ω) was evidently reduced in contrast to GQD/GCE, which was attributed to the following two major reasons: first, the co-doping of N and S atoms accelerated the electron transfer rate, and then enhanced the electroconductivity of GQD matrix so as to achieve good electrocatalytic performance; second, due to high electrical conductivity of the graphene sheets, they provided conductive substrates to interconnect the GQDs to bring about more efficient electron transport. The fast charge transfer and low resistance property of NS-GQD/G confirmed by EIS made it a competitive material for multiple electrochemical applications, specifically for electrochemical sensors.

3.2. Electrochemical performances of NS-GQD/G/GCE.

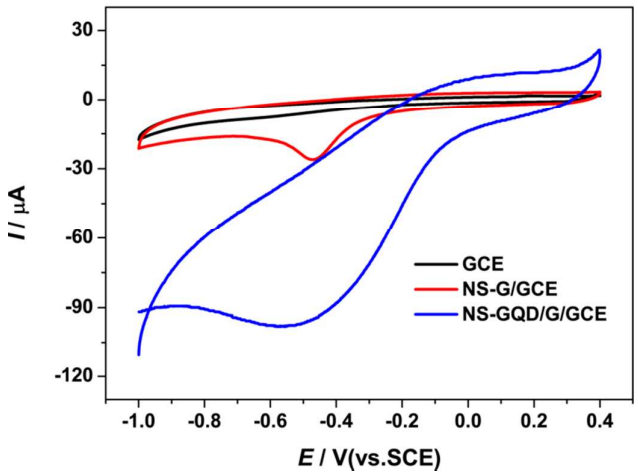

Figure 3. CV curves of 5.0 mM H_2O_2 obtained at GCE, NS-G/GCE and NS-GQD/G/GCE in N_2-saturated 0.1 M PBS (pH = 7.0) with scan rate of 50 mV s^{-1}.

Cyclic voltammetry (CV) is proverbially utilized to acquire qualitative information of various electrochemical reactions. Consequently, the electrocatalytic activity of the NS-GQD/G toward H_2O_2 reduction was estimated by CV in N_2-saturated 0.1 M PBS (pH = 7.0). Figure 3 exhibited the CV curves of the bare GCE and different materials modified GCE in the presence of 5.0 mM H_2O_2. As we can see, the blank GCE displayed poor electrocatalysis activity toward H_2O_2 reduction with inferior reduction current response. In contrast, under the identical experimental conditions, both NS-G/GCE and NS-GQD/G/GCE displayed comparatively strong reduction peaks concentrating at -0.46 V and -0.50 V, respectively. And the response currents obtained at NS-G/GCE and NS-GQD/G/GCE were about 15 times and 47 times of that obtained at bare GCE, which provided evidence that the resultant NS-G and NS-GQD/G nanomaterials possessed superduper electrocatalytic activity toward H_2O_2 reduction. In contrast to peak current obtained from G/GCE (3.8-fold increased comparing with the blank GCE) in Figure S3, it may therefore be concluded that the prominent performance of NS-G/GCE and NS-GQD/G/GCE was attributed to the introducing of N and S atoms into the graphene matrix. The N and S co-doping could

bring about numerous of topological defects and superior electron transfer ability, which would contribute to enhancing catalytic activity and boosting the conductivity of graphene. Additionally, the electrocatalytic reduction capability of NS-GQD/G/GCE was much superior than NS-G/GCE in view of their electrochemical responses, consequently, the GQDs with higher peroxidase-like activity played a decisive role in reduction performance enhancement. However, owing to the disadvantaged electroconductivity of GQDs, GQD/GCE revealed weak electrocatalytic performance with peak current improved by 1.3-fold than bare GCE. This further proved the excellent characteristics of NS-GQD/G hybrid nanocomposite. Above all, when GQDs were uniformly distributed on graphene sheets, the graphene sheets would serve as highly conductive substrates to interconnect the GQDs for efficient electron transfer. Thus the obtained NS-GQD/G could not only conquer the inferior electroconductivity of GQDs but also take full advantage of their higher peroxidase-like activity. Secondly, GQDs, abundant in oxygen-containing functional groups and exposed edges, provided more favorable conditions for dopants incorporation, bringing about the emergence of even more active sites for H_2O_2 electrocatalytic reduction. More importantly, the flake-like NS-GQD/G hybrid nanocomposite with crinkled and curved surface were loosely packed, which permitted accessible transport of supporting electrolyte and electro-reactants/products, and enhanced the electrochemical performance of NS-GQD/G. These factors together intimated NS-GQD/G hybrid nanocomposite held the post of an advanced electrochemical sensing platform to sensitively trace H_2O_2.

In the light of previous researches about the mechanism of H_2O_2 reduction on graphene based materials[46-48], the corresponding mechanism on resultant NS-GQD/G hybrid nanosheets was deduced as follows:

$$NS\text{-}GQD/G + H_2O_2 \leftrightarrow NS\text{-}GQD/G \cdot H_2O_2 \quad (1)$$

$$NS\text{-}GQD/G \cdot H_2O_2 + e^- \rightarrow NS\text{-}GQD/G \cdot (OH) + OH^- \quad (2)$$

$$NS\text{-}GQD/G \cdot (OH) + e^- \leftrightarrow NS\text{-}GQD/G + OH^- \quad (3)$$

$$H_2O_2 + 2e^- \rightarrow 2OH^- \text{ (The overall reaction)} \quad (4)$$

The first step was the adsorption of H_2O_2 on NS-GQD/G surface, forming the NS-GQD/G · H_2O_2. The second procedure was NS-GQD/G · H_2O_2 successively received two electrons, leading to the conformation of two OH^-. Simultaneously, the NS-GQD/G · H_2O_2 reverted back to NS-GQD/G at last. According to the aforementioned mechanism, it could be concluded that there were two primary limitations controlled the H_2O_2 electroreduction rate, namely, the adsorption process and the electron transfer process. Consequently, a novel material with super adsorption property and prominent electron transfer performance would be desirable for H_2O_2 detection, and NS-GQD/G hybrid nanocomposite was exactly the one that satisfied demands. First of all, heteroatom atoms doping could induce the molecular orbital localized distribution as a result of the introduction of unpaired electrons, thus leading to the weakening of O-O bond and the enhancing of H_2O_2 adsorption ability [49-50]. Secondly, given the EIS analysis, NS-GQD/G hybrid nanocomposite presented low resistance, which guaranteed its fast electron transfer property. (see Supporting Information for details) In conclusion, NS-GQD/G hybrid nanoplates were extremely suitable for H_2O_2 detection.

3.3. Effect of scan rate.

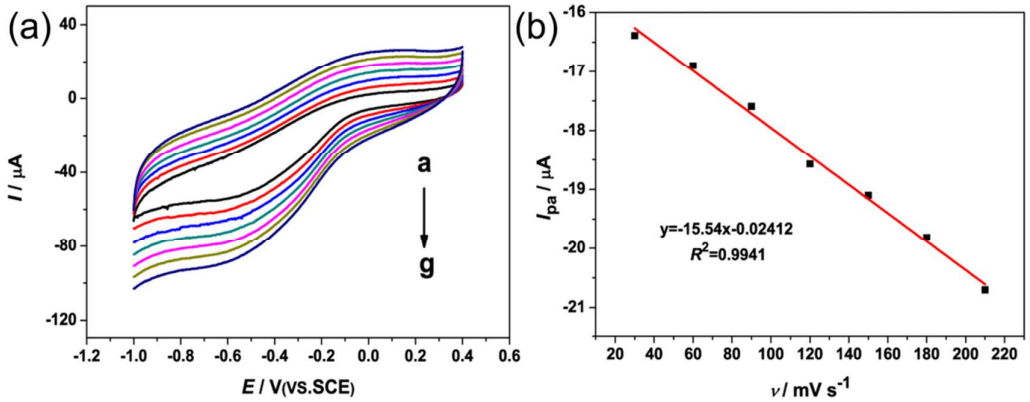

Figure 4. (a) CV curves of 1.0 mM H_2O_2 at NS-GQD/G/GCE with different scan rates in 0.1 M PBS (pH = 7.0). Curves a–g are obtained at 30, 60, 90, 120, 150, 180, 210 mV s^{-1}, respectively. **(b)** The plot of cathodic peak current (I_{pc}) vs. scan rate.

For the purpose of investigating the H_2O_2 reaction characters on NS-GQD/G modified GCE, the impact of scan rate (ν) on the H_2O_2 reduction peak current (I_{pc}) was recorded by CV measurements. As displayed in Figure 4, the I_{pc} was increased linearly with the ν ranging from 30 to 210 mV s^{-1}, and the relevant linear regression equation was I_{pc} (μA) = -15.54ν (mV s^{-1}) - 0.02412 (R^2 = 0.9941). Based on this consequent, it can be concluded that electrochemical reduction of H_2O_2 at NS-GQD/G/GCE was a representative surface-controlled process.

3.4. Amperometric determination of H_2O_2.

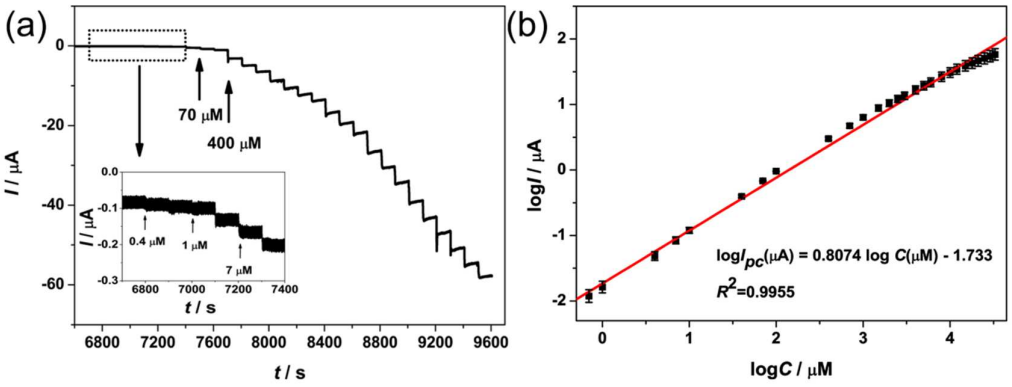

Figure 5. (a) Amperometric *i-t* curve of different concentrations of H_2O_2 in

N_2-saturated 0.1 M PBS solution (pH = 7.0) at NS-GQD/G/GCE. **(b)** The corresponding calibration curve of response current versus the concentration of H_2O_2.

Chronoamperometry was utilized to further evaluate the electrochemical performance of fabricated NS-GQD/G/GCE to H_2O_2 sensing. Figure 5a exhibited the amperometric *i-t* response of NS-GQD/G/GCE to continuing injection of varying concentrations H_2O_2 into continuously stirred deoxygenated 0.1 M PBS (pH = 7.0). -0.50 V was chose as the optimum applied potential. (see Supporting Information for details) After a certain amount of H_2O_2 was injected into the PBS, NS-GQD/G/GCE demonstrated a rapid current response as a result of the excellent electrocatalytic activity of NS-GQD/G, and the response current attained a stable state within 3 s. As displayed in Figure 5b, the logarithm of reduction current change was linear with the logarithm values of the H_2O_2 concentration ranging from 0.4 μM to 33 mM with a low detection limit of 26 nM (S/N = 3). The corresponding linear regression equation could be expressed as $\log I_{pc}$ (μA) = 0.8074 $\log C$ (μM) – 1.733 (R^2 = 0.9955). Additional similar researches about H_2O_2 electrochemical determination were summarized in Table S1 to identify the sensing performance of NS-GQD/G/GCE. In comparison with previous reported H_2O_2 sensors, our proposed NS-GQD/G/GCE sensor possessed a lower detection limit and an extended linearity range due to its excellent electrocatalytic performance and high peroxidase-like activity, particularly superior than certain horseradish peroxidase and noble metal based sensors. Therefore, NS-GQD/G/GCE would be an encouraging electrochemical sensor for accurately and sensitively monitoring H_2O_2.

3.5. Reproducibility, stability, and selectivity of NS-GQD/G/GCE.

The reproducibility of NS-GQD/G/GCE was evaluated by CV measurements. The relative standard derivation (RSD) of its reduction current response was 4.15% to ten

parallel experiments, indicating the acceptable repeatability of the proposed modified electrode.

CV measurements were also employed to examine the stability of NS-GQD/G/GCE. The NS-GQD/G/GCE maintained 90% of original current response after being kept at ambient temperature for 20 days. This revealed the satisfactory stability of NS-GQD/G/GCE.

The selectivity of NS-GQD/G/GCE to H_2O_2 sensing was researched by chronoamperometry and recorded in Figure 6. As exhibited in Figure 6, after the injection of H_2O_2, the response current changed obviously, while the response current remained unchanged when 5-fold higher concentrations of interfering substances such as glucose (GL), ascorbic acid (AA), and uric acid (UA) was added, thus testified the acceptable selectivity of NS-GQD/G/GCE. N and S atoms doping innovated unpaired electrons and further caused molecular orbital localized distribution, which weakened O-O bonds and enhanced H_2O_2 adsorption ability, giving rise to excellent selectivity of NS-GQD/G/GCE to H_2O_2 monitoring [49].

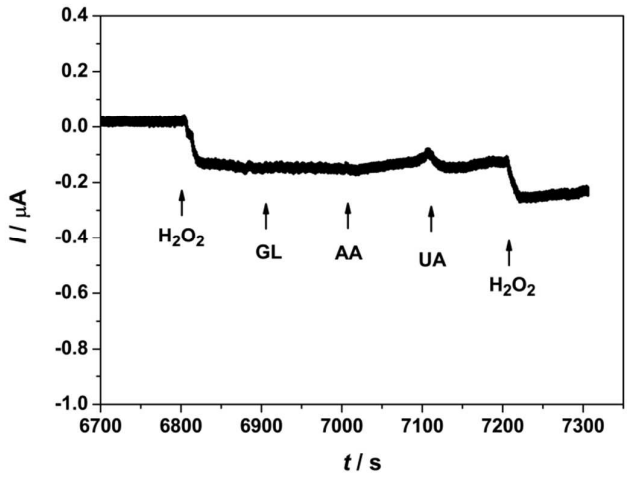

Figure 6. Amperometric response of NS-GQD/G/GCE upon sequential additions of 20 μM H_2O_2, 100 μM glucose, 100 μM ascorbic acid, 100 μM uric acid, and 20 μM H_2O_2 into constantly stirred N_2-saturated 0.1 M PBS solution.

3.6. Application in real samples.

To confirm the application feasibility of the proposed sensor to detect H_2O_2 in biological environment, standard addition method was utilized to determine H_2O_2 in human serum samples. The samples were diluted 60-times with PBS solution (pH 7.0). As listed in Table 1, the fabricated sensor exhibited satisfactory response to H_2O_2 that was spiked into the human serum, and the research results were nearly equal to their real values. In conclusion, the fabricated H_2O_2 sensor based on NS-GQD/G hybrid nanosheets presented huge application foreground in detecting H_2O_2 in physiological samples.

Table 1. Determination of H_2O_2 in real samples

Sample	Added(μM)	Found[a] (μM)	RSD (%)	Recovery (%)
Serum 1	50	47.7	2.16	95.4
Serum 2	200	208.2	1.32	104.1

[a] Average of five determinations.

3.7. Detection of H_2O_2 released from living cells.

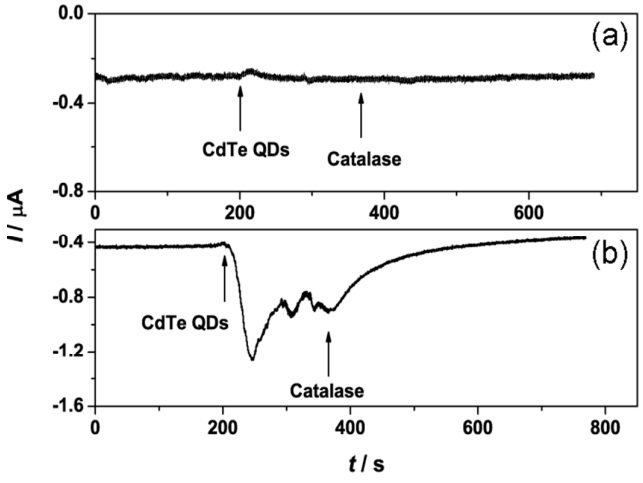

Figure 7. Amperometric responses of NS-GQD/G/GCE to the addition of 10 μL 2 mg/mL CdTe QDs with **(a)** and without **(b)** Raw 264.7 cells in N_2-saturated 0.1M

PBS (pH = 7.0).

Global cancer mortality rate has been the major cause of life-threatening public health problem, the accurate monitoring of this malignancy is of great significance. In this work, we chose Raw 264.7 cells as model cells for real-time inspecting H_2O_2 to manifest the electrochemical sensing ability of NS-GQD/G hybrid nanosheets. Raw 264.7 cells could release H_2O_2 endogenously after stimulated by CdTe QDs on base of previous reports. [51-52] As depicted in Figure 7, an obvious reduction current increase was observed upon the addition of 10 μL CdTe QDs (2.0 mg mL^{-1}) when the PBS was suspended with Raw 264.7 cells. For the purpose of confirming the current change was resulted from the H_2O_2 that generated by living cells, 50 μL of catalase (2000 U mL^{-1}) was then injected into the PBS. The corresponding current response decreased apparently and returned to the background level as a result of the decomposition of H_2O_2 induced by catalase in electrolytic solution, suggesting the current change observed in curve b was attributed to the H_2O_2 produced from the living cells. The control experiment with the absence of Raw 264.7 cells exhibited no detectable current response to the injection of CdTe QDs and catalase, further indicating the triggered H_2O_2 was the result of stimulation of cells by CdTe QDs. In conclusion, NS-GQD/G/GCE could be utilized to detect H_2O_2 generated by living cells and exhibited tremendous application prospect in physiological and pathological researches.

4. CONCLUSION

In summary, NS-GQD/G hybrid nanosheets were synthesized via facile hydrothermal reaction and thermal annealing treatment as demonstrated. The produced NS-GQD/G displayed excellent electrocatalytic performance to the electroreduction of H_2O_2 due to its efficient electrical conductivity, high

peroxidase-like activity, and enriched active sites. In view of this, NS-GQD/G nanoplates were utilized to construct a H_2O_2 biosensor. The fabricated H_2O_2 sensor exhibited an extended linear range from 0.4 μM to 33 mM, and a low detection limit down to 26 nM. In addition, researches on the reproducibility, stability, and selectivity of NS-GQD/G/GCE showed satisfactory results. More significantly, NS-GQD/G/GCE H_2O_2 sensor was smoothly used to monitor the trace amount of H_2O_2 released from living cells, which further confirmed its bright application prospect in physiological and pathological H_2O_2 biosensing.

ASSOCIATED CONTENT

Supporting Information

Synthesis of GO and GQDs. Characterization of the GO, GQDs and GQD/G. Electrochemical performances of different modified electrodes. Effect of the NS-GQD/G amount. Effect of the applied potential. **Table S1.** Comparison of reported electrodes for H2O2 determination.

AUTHOR INFORMATION

Corresponding Authors

*Email: zzq@jlu.edu.cn

*Email: hzhang@jlu.edu.cn

Notes

The authors declare no competing financial interest.

ACKNOWLEDGMENTS

Financial support by the National Natural Science Foundation of China (21375045) and Natural Science Foundation of Jilin Province (20130101118JC) is gratefully acknowledged.

References

(1) Keen, O. S.; Baik, S.; Linden, K. G.; Aga, D. S.l. Enhanced Biodegradation of Carbamazepine after Uv/H2o2 Advanced Oxidation. *Environ Sci Technol* **2012,** *46*, 11, 6222-6227.

(2) Ma, J.; Song, W.; Chen, C.; Ma, W.l. Fenton Degradation of Organic Compounds Promoted by Dyes under Visible Irradiation. *Environ Sci Technol* **2005,** *39*, 15, 5810-5815.

(3) Tsiafoulis, C. G.; Trikalitis, P. N.; Prodromidis, M. I. Synthesis, Characterization and Performance of Vanadium Hexacyanoferrate as Electrocatalyst of H2o2. *Electrochem Commun* **2005,** *7*, 12, 1398-1404.

(4) Marimuthu, T.; Mahmoudian, M. R.; Mohamad, S.; Alias, Y. Synthesis and Characterization of Non-Enzymatic Hydrogen Peroxide Sensor of Polypyrrole Coated Cobalt Nanocomposites. *Sens. Actuators, B* **2014,** *202*, 1037-1043.

(5) Shu, X.; Chen, Y.; Yuan, H.; Gao, S.l. H2o2 Sensor Based on the Room-Temperature Phosphorescence of Nano Tio2/Sio2 Composite. *Anal Chem* **2007,** *79*, 10, 3695-3702.

(6) Pramanik, D.; Dey, S. G. Active Site Environment of Heme-Bound Amyloid B Peptide Associated with Alzheimer's Disease. *J Am Chem Soc* **2011,** *133*, 1, 81-87.

(7) Wei, Y.; Zhang, Y.; Liu, Z.; Guo, M. A Novel Profluorescent Probe for Detecting Oxidative Stress Induced by Metal and H2o2 in Living Cells. *Chem Commun* **2010,** *46*, 25, 4472-4474.

(8) Yu, C.; Wang, L.; Li, W.; Zhu, C.l. Detection of Cellular H2o2 in Living Cells Based on Horseradish Peroxidase at the Interface of Au Nanoparticles Decorated Graphene Oxide. *Sens. Actuators, B* **2015,** *211*, 17-24.

(9) Almuaibed, A. M.; Townshend, A. Flow Spectrophotometric Method for Determination of Hydrogen Peroxide Using a Cation Exchanger for Preconcentration. *Anal Chim Acta* **1994,** *295*, 1, 159-163.

(10) Tanner, P. A.; Wong, A. Y. S. Spectrophotometric Determination of Hydrogen Peroxide in Rainwater. *Anal Chim Acta* **1998,** *370*, 2–3, 279-287.

(11) Ren, M.; Deng, B.; Wang, J.-Y.; Kong, X.l. A Fast Responsive Two-Photon Fluorescent Probe for Imaging H2o2 in Lysosomes with a Large Turn-on Fluorescence Signal. *Biosens Bioelectron* **2016,** *79*, 237-243.

(12) Ma, Y.; Cen, Y.; Sohail, M.; Xu, G.l. A Ratiometric Fluorescence Universal Platform Based on N, Cu Codoped Carbon Dots to Detect Metabolites Participating in H2o2-Generation Reactions. *ACS Appl Mater Interfaces* **2017,** *9*, 38, 33011-33019.

(13) Yuan, J.; Shiller, A. M. Determination of Subnanomolar Levels of Hydrogen Peroxide in Seawater by Reagent-Injection Chemiluminescence Detection. *Anal Chem* **1999,** *71*, 10, 1975-1980.

(14) Effkemann, S.; Pinkernell, U.; Karst, U. Peroxide Analysis in Laundry Detergents Using Liquid Chromatography. *Anal Chim Acta* **1998,** *363*, 1, 97-103.

(15) Song, M.; Wang, J.; Chen, B.; Wang, L. A Facile, Non-Reactive Hydrogen Peroxide (H2o2) Detection Method Enabled by Ion Chromatography with Uv Detector. *Anal Chem* **2017**.

(16) Jia, J.; Wang, B.; Wu, A.; Cheng, G.l. A Method to Construct a Third-Generation Horseradish Peroxidase Biosensor: Self-Assembling Gold Nanoparticles to Three-Dimensional Sol−Gel Network. *Anal Chem* **2002,** *74*, 9, 2217-2223.

(17) Luo, X.-L.; Xu, J.-J.; Zhang, Q.; Yang, G.-J.l. Electrochemically Deposited Chitosan Hydrogel for Horseradish Peroxidase Immobilization through Gold Nanoparticles Self-Assembly.

Biosens Bioelectron **2005,** *21*, 1, 190-196.
(18) Chen, X.; Zhang, J. J.; Xuan, J.; Zhu, J. J. Myoglobin/Gold Nanoparticles/Carbon Spheres 3-D Architecture for the Fabrication of a Novel Biosensor. *Nano Research* **2009,** *2*, 3, 210-219.
(19) Zhai, D.; Liu, B.; Shi, Y.; Pan, L.l. Highly Sensitive Glucose Sensor Based on Pt Nanoparticle/Polyaniline Hydrogel Heterostructures. *ACS Nano* **2013,** *7*, 4, 3540-3546.
(20) Meng, F.; Yan, X.; Liu, J.; Gu, J.l. Nanoporous Gold as Non-Enzymatic Sensor for Hydrogen Peroxide. *Electrochim Acta* **2011,** *56*, 12, 4657-4662.
(21) Li, Y.; Lu, Q.; Wu, S.; Wang, L.l. Hydrogen Peroxide Sensing Using Ultrathin Platinum-Coated Gold Nanoparticles with Core@Shell Structure. *Biosens Bioelectron* **2013,** *41*, 576-581.
(22) Gong, K.; Du, F.; Xia, Z.; Durstock, M.l. Nitrogen-Doped Carbon Nanotube Arrays with High Electrocatalytic Activity for Oxygen Reduction. *Science* **2009,** *323*, 5915, 760-764.
(23) Liu, H.; Liu, Y.; Zhu, D. Chemical Doping of Graphene. *J Mater Chem* **2011,** *21*, 10, 3335-3345.
(24) Geng, D.; Ding, N.; Andy Hor, T. S.; Liu, Z.l. Potential of Metal-Free "Graphene Alloy" as Electrocatalysts for Oxygen Reduction Reaction. *J Mater Chem* **2015,** *3*, 5, 1795-1810.
(25) Dai, L. Functionalization of Graphene for Efficient Energy Conversion and Storage. *Accounts Chem Res* **2013,** *46*, 1, 31-42.
(26) Nethravathi, C.; Rajamathi, C. R.; Rajamathi, M.; Gautam, U. K.l. N-Doped Graphene–Vo2(B) Nanosheet-Built 3d Flower Hybrid for Lithium Ion Battery. *ACS Appl Mater Interfaces* **2013,** *5*, 7, 2708-2714.
(27) Yang, S.; Song, X.; Zhang, P.; Gao, L. Facile Synthesis of Nitrogen-Doped Graphene–Ultrathin Mno2 Sheet Composites and Their Electrochemical Performances. *ACS Appl Mater Interfaces* **2013,** *5*, 8, 3317-3322.
(28) Dong, H.; Bai, J.; Zhu, Q.; Yu, J.l. N-Doped Graphene-Supported Pt and Pt-Ru Nanoparticles with High Electrocatalytic Activity for Methanol Oxidation. *Journal of Renewable and Sustainable Energy* **2013,** *5*, 2, 021405.
(29) Shao, Y.; Zhang, S.; Engelhard, M. H.; Li, G.l. Nitrogen-Doped Graphene and Its Electrochemical Applications. *J Mater Chem* **2010,** *20*, 35, 7491-7496.
(30) Zhao, S.; Liu, J.; Li, C.; Ji, W.l. Tunable Ternary (N, P, B)-Doped Porous Nanocarbons and Their Catalytic Properties for Oxygen Reduction Reaction. *ACS Appl Mater Interfaces* **2014,** *6*, 24, 22297-22304.
(31) Liang, J.; Jiao, Y.; Jaroniec, M.; Qiao, S. Z. Sulfur and Nitrogen Dual-Doped Mesoporous Graphene Electrocatalyst for Oxygen Reduction with Synergistically Enhanced Performance. *Angew Chem Int Ed* **2012,** *51*, 46, 11496-11500.
(32) Xu, J.; Dong, G.; Jin, C.; Huang, M.l. Sulfur and Nitrogen Co-Doped, Few-Layered Graphene Oxide as a Highly Efficient Electrocatalyst for the Oxygen-Reduction Reaction. *ChemSusChem* **2013,** *6*, 3, 493-499.
(33) Xing, T.; Zheng, Y.; Li, L. H.; Cowie, B. C. C.l. Observation of Active Sites for Oxygen Reduction Reaction on Nitrogen-Doped Multilayer Graphene. *ACS Nano* **2014,** *8*, 7, 6856-6862.
(34) Kim, H.; Lee, K.; Woo, S. I.; Jung, Y. On the Mechanism of Enhanced Oxygen Reduction Reaction in Nitrogen-Doped Graphene Nanoribbons. *Phys Chem Chem Phys* **2011,** *13*, 39, 17505-17510.
(35) Zhang, Z.; Zhang, J.; Chen, N.; Qu, L. Graphene Quantum Dots: An Emerging Material for

Energy-Related Applications and Beyond. *Energy Environ Sci* **2012,** *5*, 10, 8869-8890.
(36) Shen, J.; Zhu, Y.; Yang, X.; Li, C. Graphene Quantum Dots: Emergent Nanolights for Bioimaging, Sensors, Catalysis and Photovoltaic Devices. *Chem Commun* **2012,** *48*, 31, 3686-3699.
(37) Li, Y.; Zhao, Y.; Cheng, H.; Hu, Y.l. Nitrogen-Doped Graphene Quantum Dots with Oxygen-Rich Functional Groups. *J Am Chem Soc* **2012,** *134*, 1, 15-18.
(38) Zhang, Y.; Wu, C.; Zhou, X.; Wu, X.l. Graphene Quantum Dots/Gold Electrode and Its Application in Living Cell H2o2 Detection. *Nanoscale* **2013,** *5*, 5, 1816-1819.
(39) Tang, D.; Liu, J.; Yan, X.; Kang, L. Graphene Oxide Derived Graphene Quantum Dots with Different Photoluminescence Properties and Peroxidase-Like Catalytic Activity. *RSC Adv* **2016,** *6*, 56, 50609-50617.
(40) Wang, C.; Ma, Q.; Su, X. Synthesis of Cdte Nanocrystals with Mercaptosuccinic Acid as Stabilizer. *Journal of Nanoscience & Nanotechnology* **2008,** *8*, 9, 4408.
(41) Glenis, S.; Nelson, A. J.; Labes, M. M. Sulfur Doped Graphite Prepared Via Arc Discharge of Carbon Rods in the Presence of Thiophenes. *J Appl Phys* **1999,** *86*, 8, 4464-4466.
(42) Ciureanu, M.; Wang, H. Electrochemical Impedance Study of Electrode-Membrane Assemblies in Pem Fuel Cells I. Electro-Oxidation of H-2 and H-2/Co Mixtures on Pt-Based Gas-Diffusion Electrodes. *J Electrochem Soc* **1999,** *146*, 11, 4031-4040.
(43) Li, X.; Wang, H.; Robinson, J. T.; Sanchez, H.l. Simultaneous Nitrogen Doping and Reduction of Graphene Oxide. *J Am Chem Soc* **2009,** *131*, 43, 15939-15944.
(44) Wang, Z.; Li, P.; Chen, Y.; He, J.l. Pure Thiophene-Sulfur Doped Reduced Graphene Oxide: Synthesis, Structure, and Electrical Properties. *Nanoscale* **2014,** *6*, 13, 7281-7287.
(45) Fei, H.; Ye, R.; Ye, G.; Gong, Y.l. Boron- and Nitrogen-Doped Graphene Quantum Dots/Graphene Hybrid Nanoplatelets as Efficient Electrocatalysts for Oxygen Reduction. *ACS Nano* **2014,** *8*, 10, 10837-10843.
(46) Adić, R. R.; Marković, N. M.; Vešović, V. B. Structural Effects in Electrocatalysis. *Journal of Electroanalytical Chemistry and Interfacial Electrochemistry* **1984,** *165*, 1, 105-120.
(47) Wilshire, J.; Sawyer, D. T. Redox Chemistry of Dioxygen Species. *Accounts Chem Res* **1979,** *12*, 3, 105-110.
(48) Memming, R. Mechanism of the Electrochemical Reduction of Persulfates and Hydrogen Peroxide. *J Electrochem Soc* **1969,** *116*, 6, 785-790.
(49) Wu, P.; Du, P.; Zhang, H.; Cai, C. Microscopic Effects of the Bonding Configuration of Nitrogen-Doped Graphene on Its Reactivity toward Hydrogen Peroxide Reduction Reaction. *Phys Chem Chem Phys* **2013,** *15*, 18, 6920-6928.
(50) Zhang, T.; Li, C.; Gu, Y.; Yan, X.l. Fabrication of Novel Metal-Free "Graphene Alloy" for the Highly Efficient Electrocatalytic Reduction of H2o2. *Talanta* **2017,** *165*, 143-151.
(51) Lovrić, J.; Cho, S. J.; Winnik, F. M.; Maysinger, D. Unmodified Cadmium Telluride Quantum Dots Induce Reactive Oxygen Species Formation Leading to Multiple Organelle Damage and Cell Death. *Chem Biol* **2005,** *12*, 11, 1227-1234.
(52) Fang, H.; Pan, Y.; Shan, W.; Guo, M.l. Enhanced Nonenzymatic Sensing of Hydrogen Peroxide Released from Living Cells Based on Fe3o4/Self-Reduced Graphene Nanocomposites. *Analytical Methods* **2014,** *6*, 15, 6073-6081.

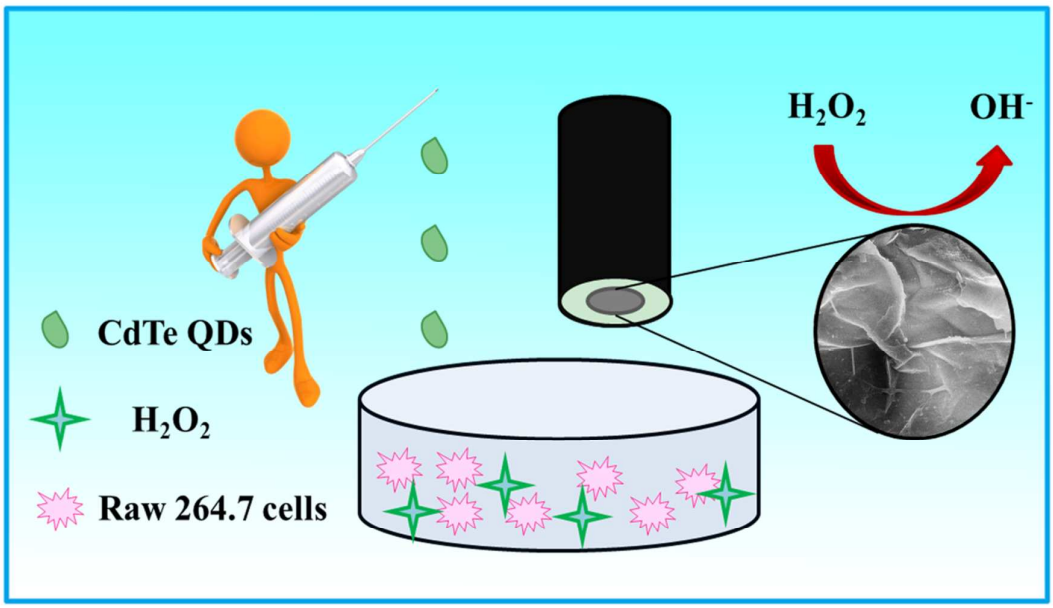

Table of Contents Graphic